

Supporting Information

for

Synthesis of urchin-like $\text{Ni}_3\text{Si}_2\text{O}_5(\text{OH})_4$ hierarchical hollow spheres/GO composite as enhanced electrochemical properties for high-performance hybrid supercapacitor

Xueying Dong¹, Yifu Zhang^{1,*}, Qiushi Wang¹, Xiaorong Zhang², Meng Gao¹, Changgong Meng¹

¹*School of Chemical Engineering, Dalian University of Technology, Dalian 116024, PR China*

²*College of Mechanical and Equipment Engineering, Hebei University of Engineering, Handan 056038, China*

*Corresponding author. E-mail address: yfzhang@dlut.edu.cn

Materials

Tetraethyl orthosilicate, ammonium hydroxide (25 wt%), nickel acetate, nickel foam, acetylene black, N-methyl-2-pyrrolidone (NMP), polyvinylidene fluoride (PVDF), graphite flakes with an average diameter of 37.4 microns, polyvinyl alcohol with an average molecular weight of 1799, and potassium hydroxide were purchased from Aladin Chemical Reagent Co., Ltd. All the chemicals were used directly without any further purification.

Synthesis of SiO₂ spheres

SiO₂ spheres with the diameter of ~300 nm were prepared based on a modified Stöber method: Under the condition of intense stirring, 2.5 mL tetraethyl orthosilicate was slowly added to 46 mL ethanol solution at a constant speed. After 10 minutes of mixing, 5 mL ammonium hydroxide was added to obtain a milky white colloidal solution. The solution was washed with ethanol and water for three times, and then dried in a vacuum drying oven for 24 hours to obtain white silica microsphere powder¹.

Synthesis of GO

The preparation method of GO was according to a modified Hummer's method, which was mainly divided into three stages: low temperature stage, medium temperature stage and high temperature stage. Low temperature stage: according to take 2 g graphite, 1g NaNO₃, 46 mL H₂SO₄, put them in 500 mL beaker, ice bathing, ultrasonic within 15 min until the beaker of solution temperature below 3 °C, transferred them to the ice bath pot then slowly added 6 g KMnO₄, stirring for 1 h to get blackening solution, the edge of the solution for the dark green; Medium temperature stages: under the condition of 35 °C water bath mixing 1 h, the solution getting into viscous significantly. High temperature stages: adding in 92 mL deionized water inside the beaker, the solution into brown, in 90 °C water bath stirring for 15 min after, then pour into 300 mL deionized water, 10 mL 30 % H₂O₂ in turn, stirring for 10 min after delamination, for the gold at the top, bottom was black, poured out on the yellow clear liquid and added 10 mL of the mass fraction of 10 % HCl, stirring again let stand for 12 h after stratification, poured out the gold solution at the top that adding deionized water until the upper supernatant fluid yellow became not obvious at this time no longer with deionized water, the GO solution was successfully prepared and turned the solution to the brown bottle for used^{2,3}.

Characterizations

The phase was confirmed by X-ray powder diffraction (XRD) using Panalytical X'Pert powder diffractometer at 40 kV and 40 mA with Ni-filtered Cu K α radiation. The chemical composition was revealed by an energy-dispersive X-ray spectrometer (EDS) and elemental mappings attached to a scanning electron microscope (SEM, QUANTA450). X-ray photoelectron spectroscopy (XPS) was performed on ESCALAB250Xi, Thermo Fisher Scientific. Fourier transform infrared spectroscopy (FTIR) pattern was measured using KBr pellet technique and recorded on a Nicolet 6700 spectrometer from 4000 to 400 cm⁻¹ with a resolution of 4 cm⁻¹. Raman spectrum was characterized by a Thermo Scientific spectrometer, with a 532 nm excitation line. The morphology was identified by field emission scanning electron microscopy (FE-SEM, NOVA NanoSEM 450, FEI) and transmission electron microscopy (TEM, FEITecna F30). Sample for FE-SEM observation was gold-sputtered in order to get better morphology, and it was dispersed in absolute ethanol with ultrasonication before TEM test. Surface area was determined by Brunauer-Emmet-Teller (BET) method using Micromeritics ASAP-2020 and the samples were degassed at 150 °C for several hours. Pore volume and average pore size were calculated by Barrett-Joyner-Halenda (BJH) formula.

Table S1**Table S1.** Synthetic condition of NiSi samples.

Sample	nickel acetate (g)	SiO ₂ (g)	Ni/Si (mole ratio)	Capacity (F g ⁻¹) at 1 A g ⁻¹
NiSi-1	0.1657	0.05	0.8/1	11
NiSi-2	0.2071	0.05	1/1	30
NiSi-3	0.3107	0.05	1.5/1	40
NiSi-4	0.4142	0.05	2/1	80
NiSi-5	0.6213	0.05	3/1	75

Temperature: 180 °C. Time: 12 h

Table S2**Table S2.** Synthetic condition of NiSi/GO samples.

Sample	NiSi (g)	GO (mL)	NiSi/GO (mass ratio)	Capacity (F g ⁻¹) at 0.5 A g ⁻¹
NiSi/GO-1	0.1	0.75	1:0.05	151
NiSi/GO-2	0.1	1.5	1:0.1	165
NiSi/GO-3	0.1	3	1:0.2	41
NiSi/GO-4	0.1	6	1:0.4	17

Water: 20 mL

Figure S1

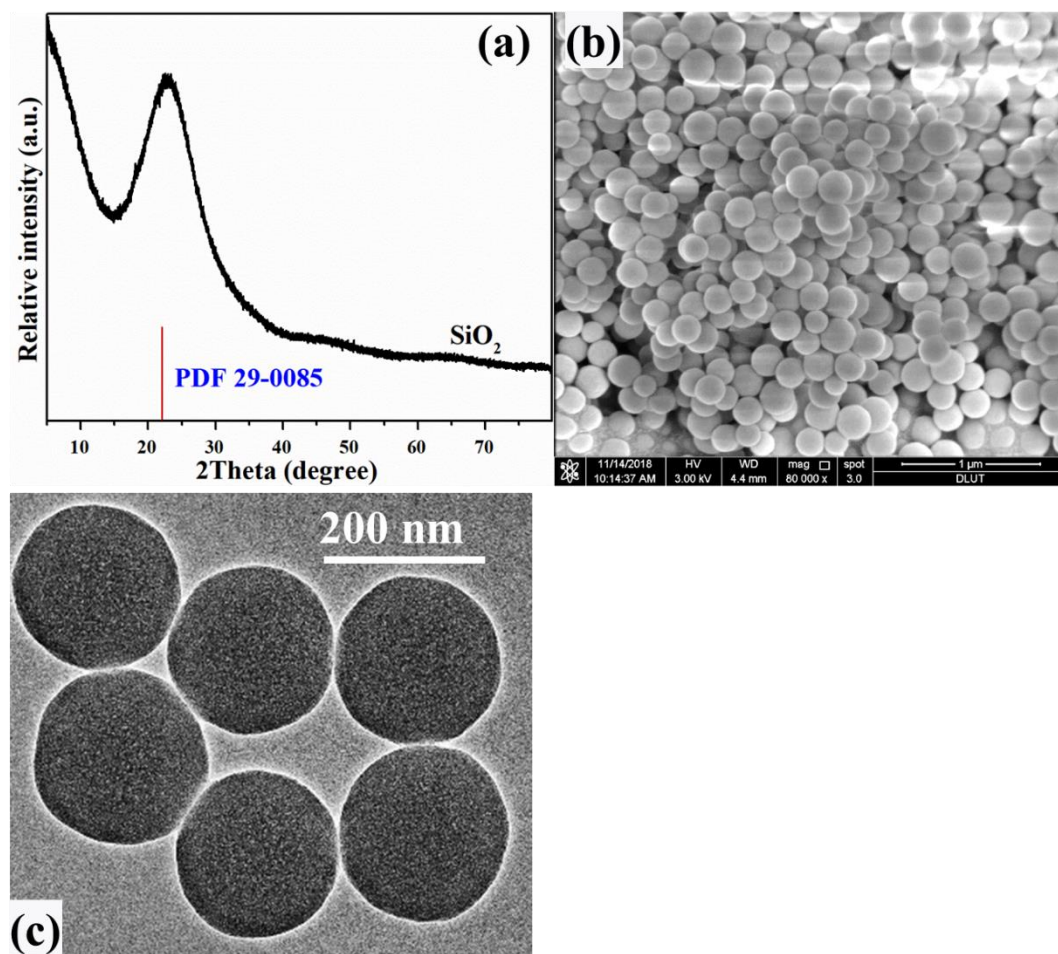


Figure S1. Characterization of SiO_2 : (a) XRD; (b) SEM; (c) TEM.

Figure S2

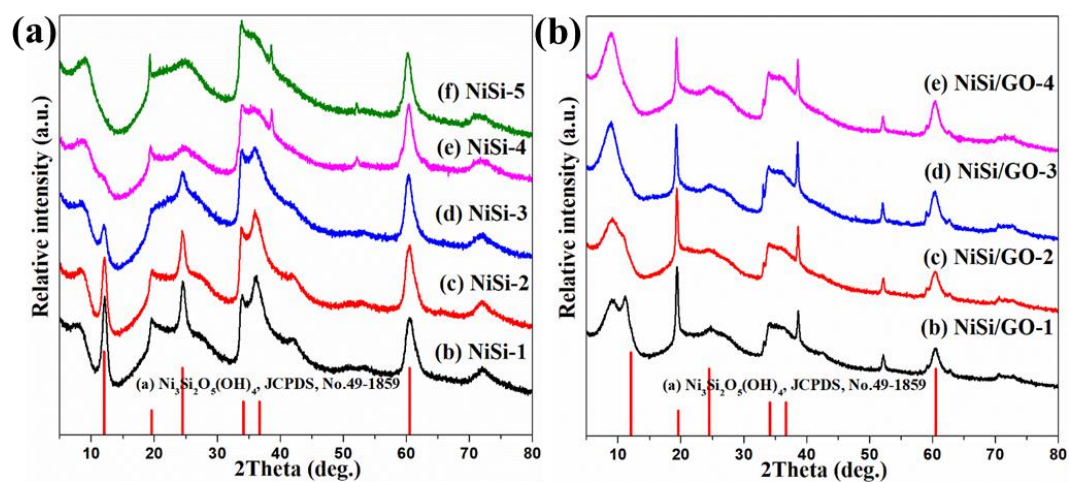


Figure S2. XRD patterns of NiSi samples (Table S1) and NiSi/GO samples (Table S2).

Figure S3

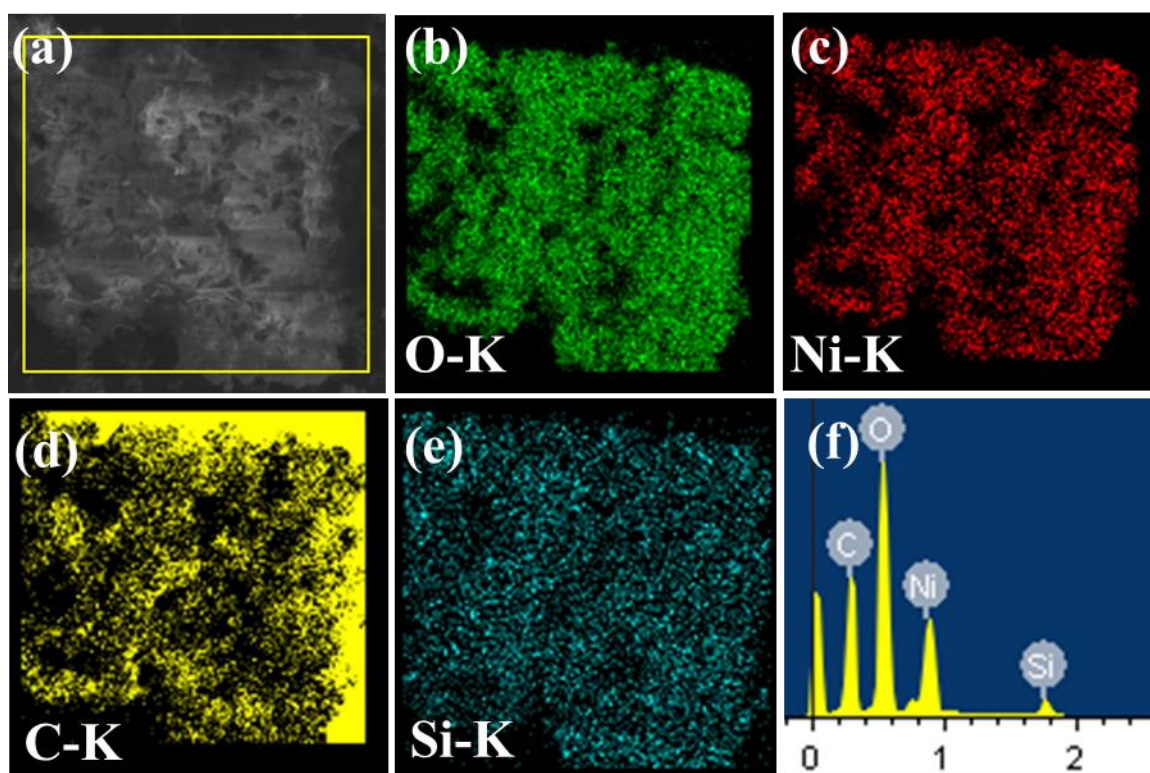


Figure S3. The composition of EDS results of NiSi/GO: (a) SEM image; (b-e) EDS mapping; (f) EDS spectrum.

Figure S4

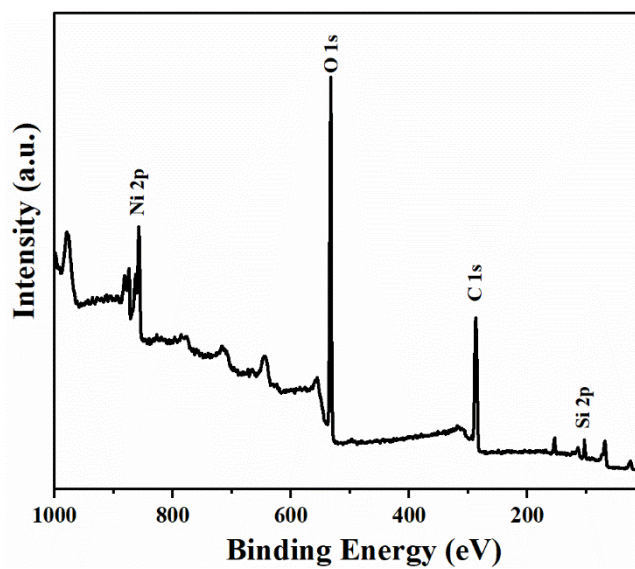


Figure S4. Full XPS spectrum of NiSi/GO.

Figure S5

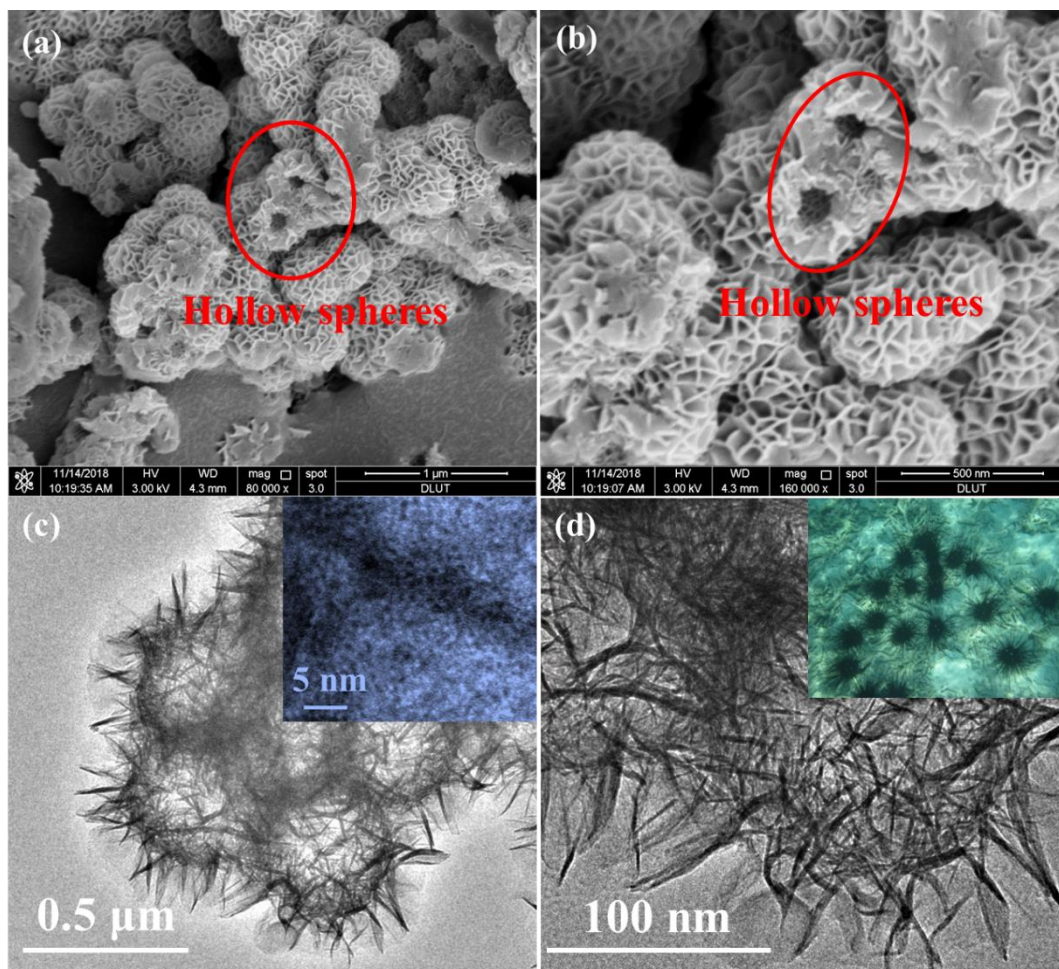


Figure S5. Morphology of the as-obtained urchin-like NiSi hollow spheres: (a-b) SEM images; (c-d) TEM images, a HRTEM image inserted in (c) and a picture of urchins inserted in (d).

Figure S6

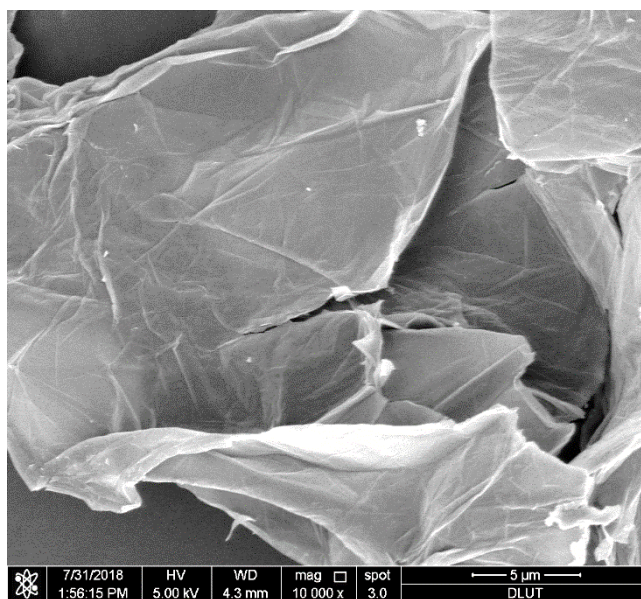


Figure S6. SEM images of GO.

Figure S7

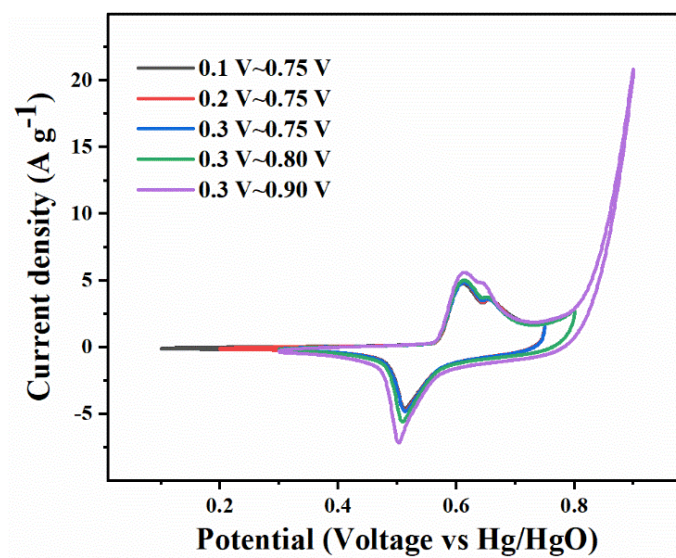


Figure S7. CV curves of NiSi hollow spheres on various potential limits at the scan rate of $20\ mV\ s^{-1}$.

Figure S8

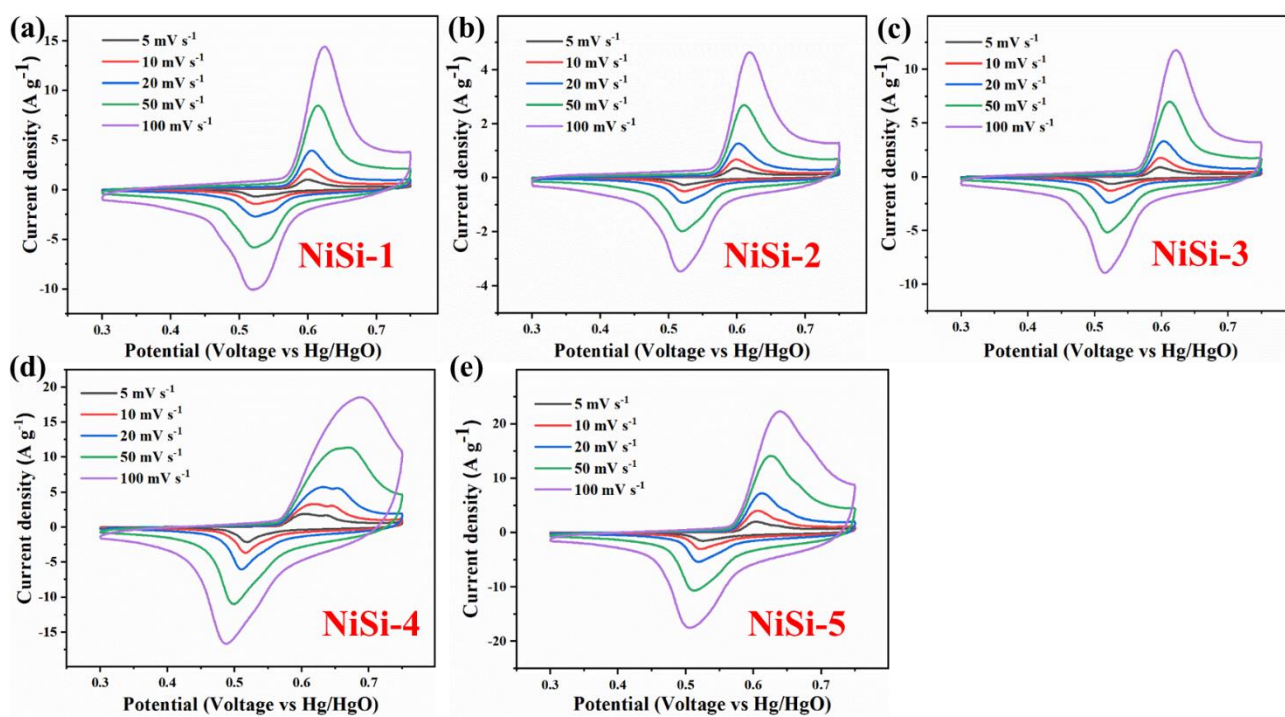


Figure S8. CV curves of NiSi synthesized by various conditions (see Table S1) at different scan rates.

Figure S9

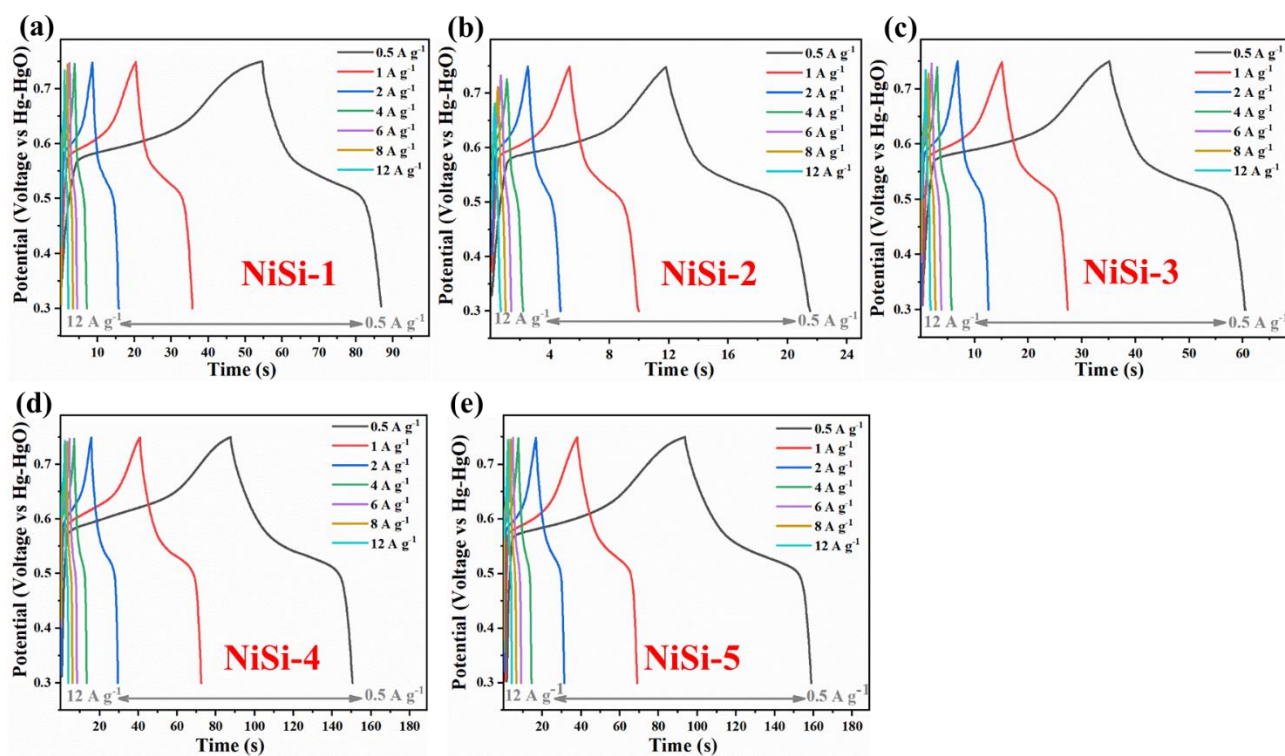


Figure S9. GCD curves of NiSi synthesized by various conditions (see Table S1) at different current densities.

Figure S10

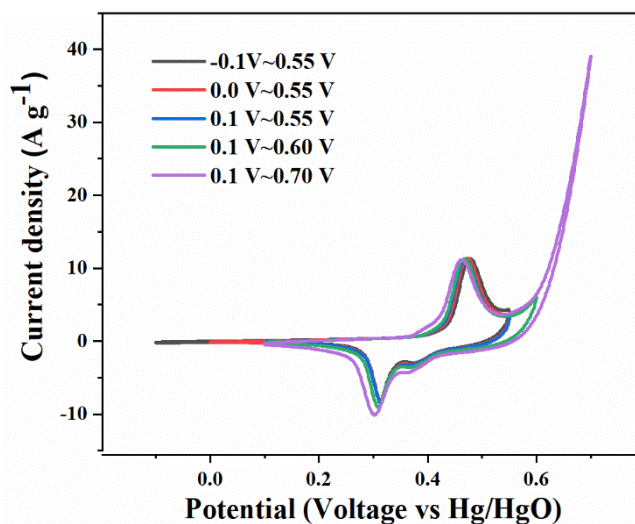


Figure S10. CV curves of NiSi/GO on various potential limits at the scan rate of 20 mV s⁻¹.

Figure S11

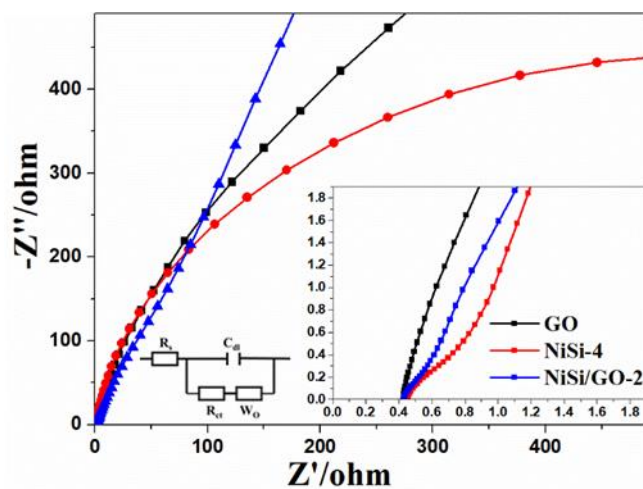


Figure S11. Nyquist plots and equivalent electrical circuit of GO, NiSi-4, NiSi/GO-2.

Figure S12

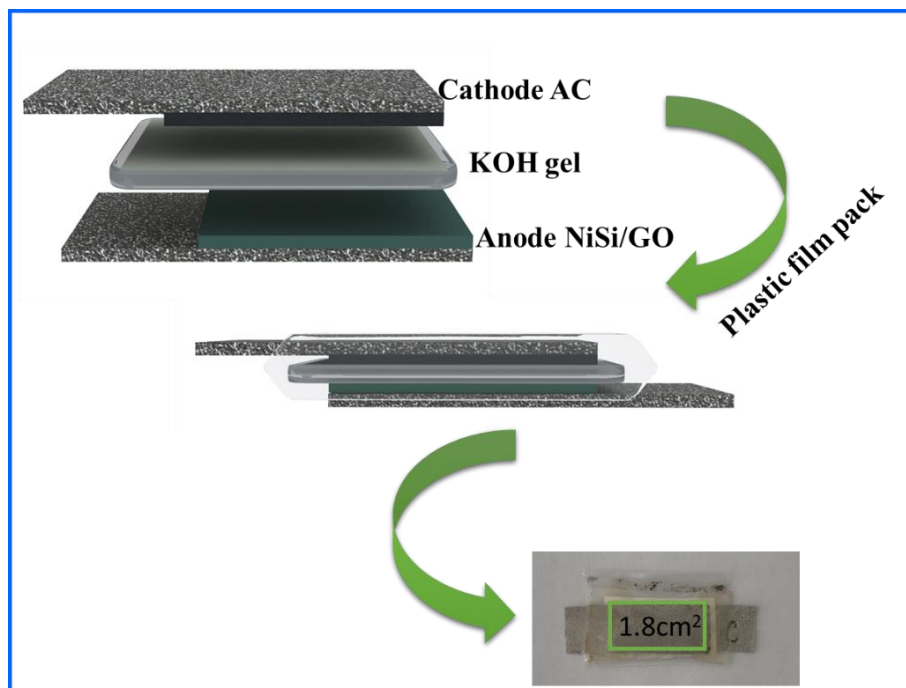


Figure S12. Schematic diagram of fabricating NiSi/GO//AC HSC device.

Figure S13

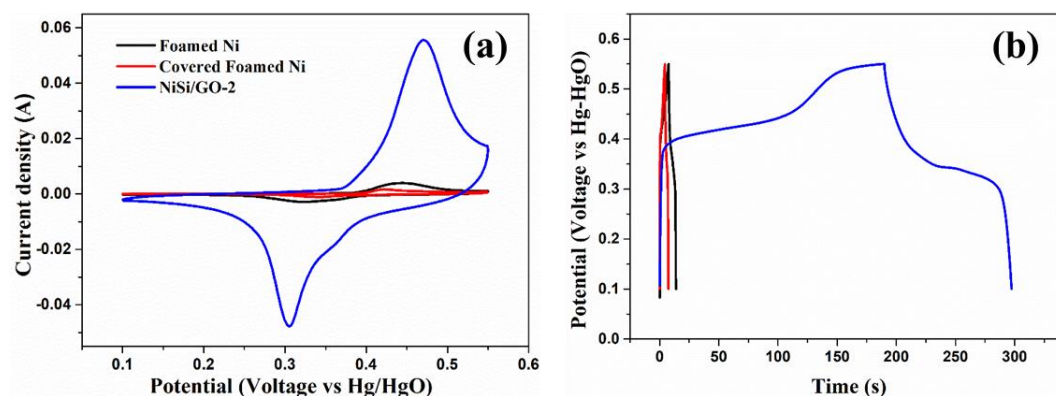


Figure S13. (a) CV curves of NiSi/GO-2, Foamed Ni and Foamed Ni covered with electrode paste without active material at the scan rate of 20 mV s^{-1} and (b) GCD curves of NiSi/GO-2, Foamed Ni and Foamed Ni covered with electrode paste without active material (the current agrees the current density of NiSi/GO-2 at 0.5 A g^{-1}).

The effect of nickel foam in the present work can be ignored in our system based on the following reasons.

First, the contribution of the capacitance of nickel foam is small. In order to explore how much electrical capacity nickel foam would contribute to our system, we were carried out a controlled trial. Under the same experimental conditions, we respectively tested the CV and GCD curves of nickel foam and nickel foam whose surface was covered by electrode paste (excluding active substances), as shown in Figure S13. Nickel foam contributes about 7 F/g at 0.5 A/g . However, when the surface of nickel foam is covered, the capacitance is only about 3.5 F/g . Thus, accounting for about 2% of the total capacity, the effect is so small that it can be ignored in this system.

Second, the electrochemical process of supercapacitors mainly occurs at the surface. Once the surface of foamed nickel is coated, its ability to participate in electrochemical reactions decreases. The previous reports demonstrated that small mass loading can cause huge error if the mass loading is less than 1 mg/cm^2 ⁴⁻⁶. If the mass loading is over 1 mg , the results are acceptable. In this work, the mass loading of the active materials was ca. $3\text{-}4 \text{ mg/cm}^2$, thus the impact of such a large mass loading and the covered nickel foam in the system could be ignored, in agreement with the report of Zhou⁵.

Third, in recent years, there are still advanced research groups using nickel foam as a collector for alkaline electrolyte, and achieved good performance ⁷⁻¹⁰.

Based on above statements, this manuscript using nickel foam as current collectors with high mass loading to evaluate electrochemical performance in alkaline electrolyte should be acceptable.

Table S3

Table S3. Comparison of the electrochemical performance of various supercapacitor devices.

Devices	Electrolyte	Potential/ V	Capacitance /mF cm ⁻²	Energy density	Power density	Cycling capability	Ref.
RGO/Cellulose SSC	H ₂ SO ₄ /PV A	0~0.8	46, 2 mV s ⁻¹	15 μWh cm ⁻²	–	99 % after 5000	11
Activated carbon cloth SSC	H ₂ SO ₄ /PV A	0~1	31, 10 mV s ⁻¹	–	–	95 % after 20000	12
Graphene-cellulose tissue composites SSC	H ₂ SO ₄ /PV A	0~1.1	80	9 μWh cm ⁻²	100 mW cm ⁻²	90 % after 5000	13
Hierarchical carbon tubular nanostructures SSC	H ₃ PO ₄ /PV A	0~1	80, 5 mV s ⁻¹	–	–	–	14
Hierarchical carbon tubular nanostructures SSC	KOH/PVA	0~1	79, 5 mV s ⁻¹	–	–	–	14
Graphite nanosheets/PANI SSC	H ₂ SO ₄ /PV A	0~0.8	77.8, 0.1 mA cm ⁻²	–	–	83 % after 10000	15
CoSi hollow sphere//AC HSC	KOH/PVA	0~1.5	375.5, 2 mA cm ⁻²	2.6 mWh cm ⁻³ (11.5 W h kg ⁻¹)	-	45 % after 2800	1
MnSi hollow sphere//AC HSC	KOH/PVA	0~1.2	1048.3, 2 mA cm ⁻²	4.6 mWh cm ⁻³ (9.7 W h kg ⁻¹)	-	32 % after 900	1
NiSi hollow sphere//AC HSC	KOH/PVA	0~1.6	120.9, 2 mA cm ⁻²	0.93 mWh cm ⁻³ (3.78 W h kg ⁻¹)	-	42 % after 3000	1
PET/Pt/MnO ₂ SSC	H ₃ PO ₄ /PV A	0~0.8	20, 10 mV s ⁻²	1.9*10 ⁻⁶ Wh cm ⁻²	1.6*10 ⁻⁴ W cm ⁻²	82.2 % after 10000	16
V ₂ O ₅ H ₂ O/graphene SSC	LiCl/PVA	-0.8~0.8	12, 0.25 A m ⁻²	1.14 μW h cm ⁻²	10.0 μW cm ⁻²	95 % after 2000	17
VO ₂ NF@3DG SSC	K ₂ SO ₄	-0.6~0.6	70.8, 0.5 mA cm ⁻²	279.6 mWh m ⁻²	6000 mW m ⁻²	64 % after 3000	18
3D C-ZnSi//AC HSCs	KOH/PVA	0~1.6	194, 2 mA cm ⁻²	0.69 Wh m ⁻²	8 W m ⁻²	80 % after 6900	19
MnSi-C-3//Ni(OH) ₂ ASC	KOH/PVA	0~2	438.5, 4 mA cm ⁻²	5.3 mWh cm ⁻³ (24.6 Wh kg ⁻¹)	130.4 mW cm ⁻³ (604.8 W kg ⁻¹)	34 % after 1000	20
NiCo ₂ O ₄ SSCs	KOH/PVA	0~1	160, 1 mA cm ⁻²	-	-	-	21
VC@C SSC device	LiCl/PVA	0~0.8	46, 5 mV s ⁻¹	0.024 Wh m ⁻²	0.8 W m ⁻²	81 % after 2000	22
VN@C SSC device	LiCl/PVA	0~0.8	65, 5 mV s ⁻¹	0.041 Wh m ⁻²	0.8 W m ⁻²	85 % after 2000	22
NiSi/GO//AC HSC device	KOH/PVA	0~1.55	109 (18 F g ⁻¹) at 1 mA cm ⁻²	0.37 Wh m ⁻² (6 W h kg ⁻¹)	1.94 W m ⁻² (31.8 W kg ⁻¹)	71% after 5000 cycles	This work

HSCs = Hybrid Supercapacitors; ASC = Asymmetric Supercapacitors; SSCs = Symmetric Supercapacitors.

References

1. Q. S. Wang, Y. F. Zhang, H. M. Jiang, X. J. Li, Y. Cheng and C. G. Meng, *Chem Eng J*, 2019, **362**, 818-829.
2. M. Chen, Y. Zhang, Y. Liu, Q. Wang, J. Zheng and C. Meng, *ACS Appl. Energy Mater.*, 2018, **1**, 5527-5538.
3. T. Hu, Y. Liu, Y. Zhang, M. Chen, J. Zheng, J. Tang and C. Meng, *J. Colloid Interface Sci.*, 2018, **531**, 382-393.
4. M. Grdeń, M. Alsabet and G. Jerkiewicz, *ACS Appl. Mater. Interfaces*, 2012, **4**, 3012-3021.
5. W. Xing, S. Qiao, X. Wu, X. Gao, J. Zhou, S. Zhuo, S. B. Hartono and D. Hulicova-Jurcakova, *J. Power Sources*, 2011, **196**, 4123-4127.
6. R. B. Rakhi, W. Chen, D. Cha and H. N. Alshareef, *Nano Lett.*, 2012, **12**, 2559-2567.
7. L. Hou, Y. Shi, C. Wu, Y. Zhang, Y. Ma, X. Sun, J. Sun, X. Zhang and C. Yuan, *Adv. Funct. Mater.*, 2018, **28**, 1705921.
8. W. Kong, C. Lu, W. Zhang, J. Pu and Z. Wang, *J. Mater. Chem. A*, 2015, **3**, 12452-12460.
9. R. Kumar, P. Rai and A. Sharma, *J. Mater. Chem. A*, 2016, **4**, 9822-9831.
10. K. Xu, W. Li, Q. Liu, B. Li, X. Liu, L. An, Z. Chen, R. Zou and J. Hu, *J. Mater. Chem. A*, 2014, **2**, 4795-4802.
11. Z. Weng, Y. Su, D.-W. Wang, F. Li, J. Du and H.-M. Cheng, *Adv. Energy Mater.*, 2011, **1**, 917-922.
12. G. Wang, H. Wang, X. Lu, Y. Ling, M. Yu, T. Zhai, Y. Tong and Y. Li, *Adv. Mater.*, 2014, **26**, 2676-2682.
13. M. Sevilla, G. A. Ferrero and A. B. Fuertes, *Energy Storage Mater. (Netherlands)*, 2016, **5**, 33-42.
14. H. Zhang, H. Su, L. Zhang, B. Zhang, F. Chun, X. Chu, W. He and W. Yang, *J. Power Sources*, 2016, **331**, 332-339.
15. B. Yao, L. Yuan, X. Xiao, J. Zhang, Y. Qi, J. Zhou, J. Zhou, B. Hu and W. Chen, *Nano Energy*, 2013, **2**, 1071-1078.
16. X. Long, Z. Zeng, E. Guo, X. Shi, H. Zhou and X. Wang, *J. Power Sources*, 2016, **325**, 264-272.
17. J. Bao, X. Zhang, L. Bai, W. Bai, M. Zhou, J. Xie, M. Guan, J. Zhou and Y. Xie, *J. Mater. Chem. A*, 2014, **2**, 10876-10881.
18. J. Wang, X. Zhang, Y. Zhang, A. Abas, X. Zhao, Z. Yang, Q. Su, W. Lan and E. Xie, *RSC Adv.*, 2017, **7**, 35558-35564.
19. Y. F. Zhang, H. M. Jiang, Q. S. Wang and C. G. Meng, *Chem Eng J*, 2018, **352**, 519-529.
20. Q. S. Wang, Y. F. Zhang, H. M. Jiang and C. G. Meng, *J Colloid Interf Sci*, 2019, **534**, 142-155.
21. Q. F. Wang, X. F. Wang, B. Liu, G. Yu, X. J. Hou, D. Chen and G. Z. Shen, *J Mater Chem A*, 2013, **1**, 2468-2473.
22. Y. Zhang, J. Zheng, X. Jing and C. Meng, *Dalton Trans.*, 2018, **47**, 8052-8062.